This is a repository copy of *Strong coupling in molecular systems: a simple predictor employing routine optical measurements*.

White Rose Research Online URL for this paper:
https://eprints.whiterose.ac.uk/213307/

Version: Published Version

Research Article

Marie S. Rider, Edwin C. Johnson, Demetris Bates, William P. Wardley, Robert H. Gordon, Robert D. J. Oliver, Steven P. Armes, Graham J. Leggett and William L. Barnes*

Strong coupling in molecular systems: a simple predictor employing routine optical measurements

Abstract: We provide a simple method that enables readily acquired experimental data to be used to predict whether or not a candidate molecular material may exhibit strong coupling. Specifically, we explore the relationship between the hybrid molecular/photonic (polaritonic) states and the bulk optical response of the molecular material. For a given material, this approach enables a prediction of the maximum extent of strong coupling (vacuum Rabi splitting), irrespective of the nature of the confined light field. We provide formulae for the upper limit of the splitting in terms of the molar absorption coefficient, the attenuation coefficient, the extinction coefficient (imaginary part of the refractive index) and the absorbance. To illustrate this approach, we provide a number of examples, and we also discuss some of the limitations of our approach.

*Corresponding author: William L. Barnes, Department of Physics and Astronomy, University of Exeter, Stocker Road, Devon EX4 4QL, UK, E-mail: W.L.Barnes@exeter.ac.uk. https://orcid.org/0000-0002-9474-5534
Marie S. Rider and William P. Wardley, Department of Physics and Astronomy, University of Exeter, Stocker Road, Devon EX4 4QL, UK, E-mail: M.S.Rider@exeter.ac.uk (M. S. Rider), W.Wardley@exeter.ac.uk (W. P. Wardley). https://orcid.org/0000-0001-5130-1901 (M. S. Rider), https://orcid.org/0000-0001-9194-5154 (W. P. Wardley)
Edwin C. Johnson, **Demetris Bates**, **Steven P. Armes and Graham J. Leggett**, Department of Chemistry, University of Sheffield, Brook Hill, Sheffield, S3 7HF, UK, E-mail e.c.johnson@sheffield.ac.uk (E. C. Johnson), d.bates@sheffield.ac.uk (D. Bates), s.p.armes@sheffield.ac.uk (S. P. Armes), graham.leggett@sheffield.ac.uk (G. J. Leggett). https://orcid.org/0000-0002-0092-1008 (E. C. Johnson)
Robert H. Gordon, Department of Physics and Astronomy, University of Sheffield, Hicks Building, Hounsfield Road, Sheffield, S3 7RH, UK, E-mail rhgordon1@sheffield.ac.uk
Robert D. J. Oliver, Department of Physics and Astronomy, University of Sheffield, Hicks Building, Hounsfield Road, Sheffield, S3 7RH, UK; and Department of Materials Science and Engineering, University of Sheffield, Sir Robert Hadfield Building, Mappin Street, Sheffield, S1 3JD, UK, E-mail: robert.oliver@sheffield.ac.uk

1 Introduction

Coupling of a vibrational or an excitonic resonance of an ensemble of molecules to an optical cavity mode (confined light field) has become a major area of research. Interest is focused in particular on what happens when the coupling between the molecules and the confined light field enters the strong coupling regime [1], [2]. In this regime, the molecular resonance at (angular) frequency ω_0 hybridises with an optical resonance (e.g. that of an optical microcavity [3]) to produce two new modes – polaritons – that are part light, and part molecular resonance, at frequencies ω_+ (upper polariton) and ω_- (lower polariton). The difference in frequency (energy) of the upper and lower polaritons at resonance is usually called the Rabi frequency and, since we often wish to know how far from the original molecular resonance, ω_0, the two polaritons $\omega_\pm$ are, we write $\Omega_R = \omega_+ - \omega_- = 2g_N$ where g_N is the N-molecule interaction strength [2], see Figure 1. The extent of the hybridisation can be so dramatic that the associated energy levels may be shifted by a substantial fraction of the unperturbed resonance energy [4]. Interest is particularly strong from the perspective of using molecular strong coupling to modify energy transport between molecules [5], [6], to control exciton transport [7] and to alter chemical reactions [1], although the extent to which this is possible is still an area of vigorous debate [8]–[13].

Various theoretical and computational approaches can be adopted both to explore and understand the associated phenomena [14], [15], ranging from simple classical oscillator models [2] to sophisticated macroscopic quantum electrodynamics [16] and ab-initio numerical quantum chemistry approaches [17], [18]. Classical models are remarkably effective, and simple mechanical coupled oscillator models and transfer matrix approaches are particularly prevalent
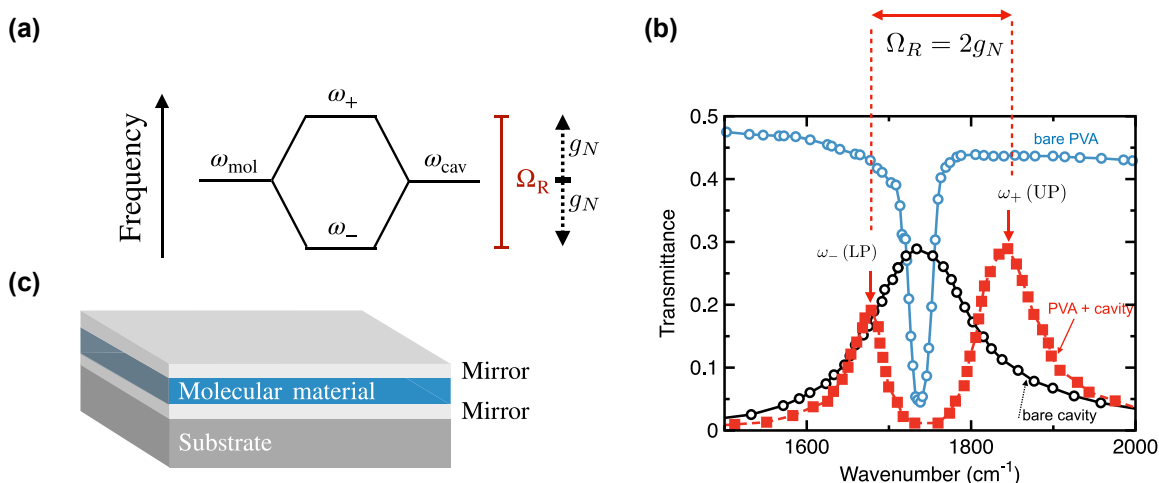
(a)

(c)

(b)

Figure 1: Overview of molecular strong coupling (a) Strong coupling between a molecular resonance and a cavity resonance results in two new hybrid energy levels separated by frequency $\Omega_R = \omega_+ - \omega_- = 2g_N$. (b) This hybridisation and resultant energy level splitting can be seen in the transmission of the system, here employing data adapted from Shalabney et al. [50]. The blue data are the transmittance of a polymer (polyvinyl acetate, PVA) film in the absence of a cavity. The strong absorption at ~1730 cm^{-1} is due to the C=O stretch mode in the PVA. The black data show the transmittance of an empty cavity, i.e. one in which the oscillator strength associated with the molecular resonance has been set to zero. The red data show that when the cavity is filled with PVA, the original single transmission peak is lost and two new transmittance peaks emerge, the upper (ω_+) and lower (ω_-) polaritons. (c) The molecule-cavity system we consider is that of a polymer sandwiched between two mirrors.

in the literature and often seem to successfully account for observed phenomena [19], [20].

Both the dispersion of the split modes (polaritons) and the extent of the Rabi splitting (shown in Figure 1(b)) can be predicted solely on the basis of a detailed knowledge of the bulk optical response of the molecular material involved, for example that of the dye-doped polymer used to fill the cavity shown in Figure 1(c). This approach to modelling strong coupling has been successfully used in the context of phonon resonances [21]. Here, we investigate these ideas in the context of molecular excitonic and vibrational resonances, for example dye-doped polymers. We focus our attention on how the results of simple optical measurements can be harnessed in a predictive way to help in the design of molecular strong coupling systems. To keep the message of the main text clear, we restrict the majority of derivations to the appendices.

2 Summary of key formulae

2.1 Strong coupling criterion

Whether or not one can expect strong coupling to be observed depends on whether the interaction strength (rate) between the molecular resonators and the confined light field exceeds the dissipation rates. We can also consider this condition from a spectroscopic viewpoint: we need the

Rabi frequency, Ω_R, to exceed the mean of the cavity, K, and molecular, Γ, linewidths. Noting that the Rabi frequency is twice the interaction strength, then for strong coupling, we have the following condition [2],

$$\Omega_R = 2g_N > \frac{\Gamma + K}{2}. \tag{1}$$

A fuller discussion of strong coupling criteria is given in Appendix A.

We focus here on calculating a value for g_N from experimentally measurable parameters. We can see from (1) that strong coupling is possible provided $\Omega_R - \Gamma$ is positive; if it is then we can rearrange equation (1) to set a *usable* upper bound on the cavity linewidth, K, for which strong coupling can be observed, specifically,

$$K < 2\Omega_R - \Gamma. \tag{2}$$

2.2 Interaction strength

The strength of the interaction of N molecular resonators and a cavity mode, g_N, is based on the electric dipole interaction. We consider molecular resonances that involve electric dipole transitions, at angular frequency, ω_0, and that have a transition dipole moment, μ. Note that the formation of polariton modes involves the interaction of this dipole moment with the cavity vacuum field, E_{vac}. No external source of light is involved in the formation of these new, coupled modes. Observation of the modes will usually involve

light, but the modes exist whether or not the cavity is illuminated [1], [2].

The interaction energy for a single electric dipole is given by,

$$\hbar g = \mu . E_{\text{vac}}, \tag{3}$$

where we have assumed that the dipole moment and field are aligned. The (RMS) strength of the vacuum field is $\sqrt{\hbar\omega_0/2V_m\varepsilon_0\varepsilon_{\text{host}}}$, where $\varepsilon_{\text{host}}$ is the background permittivity of the molecular material, and V_m is the volume of the cavity mode [2]. For example, the mode volume associated with the plasmon mode of a gold nanosphere will be roughly the surface area of the sphere multiplied by the decay length of the electric field associated with the plasmon mode into the surrounding medium [22]. As another example, the mode volume associated with an optical microcavity will be roughly the cavity thickness multiplied by the area of the mode, which in turn is dictated by the spatial coherence properties of the mode [23]. Calculating exact mode volumes is a subtle business [24], but we only need to appreciate the underlying ideas involved here, there is also the question of whether the molecules of interest fill the mode volume, a matter we discuss in the third bullet point bellow. The last piece of information we need is that the interaction energy scales as the square root of the number of dipoles (molecules) involved [2]. We thus have,

$$g_N = \left(\frac{\Omega_R}{2}\right) = \frac{1}{\hbar}\sqrt{N}\mu E_{\text{vac}} = \frac{1}{\hbar}\sqrt{N}\mu\sqrt{\frac{\hbar\omega_0}{2V_m\,\varepsilon_0\,\varepsilon_{\text{host}}}}. \tag{4}$$

Whether or not this value of g_N is sufficient for strong coupling to be observed depends on whether the strong coupling condition, equation (1) is met.

Equations (1) and (4) are standard results, but they are not convenient if one wishes to make an estimate as to whether a particular molecular resonance/material combination will yield strong coupling. To see why we can rearrange equation (4) to write the coupling energy, E_C, in terms of the coupling strength g_N as,

$$E_C = \hbar g_N = \sqrt{\frac{\mu^2 E_0 N}{2\varepsilon_0\varepsilon_{\text{host}}V_m}}, \tag{5}$$

where E_0 is the energy of the molecular resonance and is assumed to be matched to the resonance frequency of the cavity. Our result, (5), is similar to that of [25], [26]; we note, however, that the exact form of this expression relies on the system of units used, the assumed spatial variation of the cavity field and the distribution and orientation of the molecules within the cavity. If we know the dipole moment, μ, and we also know the number density of molecular resonators in the cavity, N/V_m, then the interaction

strength is easily determined. However, N/V_m, and in particular μ, are not easily derived from standard experimental measurements, although it can be done, see Appendix B and also [27].

In what follows we reformulate equation (4) in a number of ways so as to more easily facilitate strong coupling predictions based on common measurements of material properties.

We show in Appendices C and D, that the interaction strength in terms of the extinction coefficient κ (equal to the imaginary part of the complex refractive index) of a thin solid layer of material (or a cuvette of material in solution) can be found using the following procedure:

- We assume that the molecular resonance can be described as a Lorentzian oscillator (LO).
- We use the LO model to write the interaction strength in terms of an oscillator strength for the transition, rather than a dipole moment.
- The LO model then allows us to obtain the permittivity of the material, $\varepsilon(\omega)$, and from $\varepsilon(\omega)$ we can extract the extinction coefficient (the imaginary part of the (complex) refractive index $n + i\kappa$) through $(n + i\kappa)^2 = \varepsilon$.

Details are given in Appendices C and D; the result is that the interaction strength in terms of the peak (maximum) value of the extinction coefficient κ can be approximated as,

$$g_N = \frac{0.56}{\sqrt{n_{\text{host}}}}\sqrt{\kappa_{\max}\,\omega_0\,\delta\omega}, \tag{6}$$

where, for clarity, $\kappa_{\max}$ is the maximum value of the extinction coefficient associated with the molecular transition, ω_0 is the (angular) frequency of the molecular transition (rad s^{-1}), $\delta\omega$ is the width of the extinction feature (rad s^{-1}) and n_{host} is the background refractive index of the molecular host (e.g. solvent or polymer). For practical purposes – see Appendix A – we take $\Gamma \approx \delta\omega$ if we are working in rad s^{-1}, and $\Gamma \approx \delta\bar{\nu}$ or $\Gamma \approx \delta E$ if we are working in cm^{-1} or eV, respectively.

We note a number of assumptions that we have made:

- We have assumed that the dipole moments of the molecules are randomly oriented. If instead they were oriented, for example, in the direction of the E-field of the light, then we would need to multiply the right-hand side of (6) by $\sqrt{3}$.
- The question of how best to incorporate inhomogeneous broadening is on-going, e.g. via various modified forms of the LO model [28]–[30]. In Appendix D, the final form of equation (6) is based on relaxing the assumption that the description of the transition

should be Lorentzian, we use a generalised spectroscopic approach [31].

- We have also implicitly assumed that the molecules of interest fill the mode volume. For a closed Fabry–Pèrot cavity, this may be a good approximation, but in other situations, this may not be the case, e.g. a monolayer of molecules on a metal surface that supports a surface plasmon mode, or on a metallic particle [32]. Investigating the effect of only partially filling the mode volume is beyond the scope of the present study; our calculations provide a 'best case' in this regard.

We note that Gunasekaran et al. have used a related approach to extract predictive information from absorption spectra [33]. In Table 1, we provide equivalent formulae in terms of a number of different common spectral parameters, and we do so for a variety of spectral units: (i) wavenumber ($\bar{\nu}$), in cm^{-1}; (ii) angular frequency ω, in radians s^{-1} and (iii) electron volts (eV); details are given in the appendices. Note that these parameters are all frequencies, or equivalent. Frequently experimental data are acquired in terms of wavelength, e.g. from a UV–VIS (ultraviolet-visible) spectrophotometer. In this case, the data need to be converted to frequency to avoid lineshape distortion [34]; furthermore, making direct use of transmittance to determine

Table 1: Formulae for the maximum interaction strength, g_N, in terms of material parameters. Equations are given (by row) for four different material parameters: molar absorption coefficient ϵ; absorption coefficient α; extinction coefficient κ and absorbance (a) (equivalent to optical density (OD)), and by column for different units: wavenumber $\bar{\nu}$ (cm^{-1}); angular frequency ω (rad s^{-1}) and energy E (eV). In each column, the prefactors for the equations are set so as to yield the coupling strength in the same units. Thus, for the wavenumber column, using the equations given above will yield a coupling strength in wavenumbers (cm^{-1}) etc. It is important to note the units used here, we have tried to adopt the conventions used in practice. Accordingly, for the top row the molar absorption coefficient, ϵ, is in units of dm^3 mol^{-1} cm^{-1}, whilst the concentration, C, is in units of mol dm^{-3}. For the second row, the attenuation coefficient is in units of cm^{-1}. For the third row, the extinction coefficient, κ, is dimensionless and has no units. In the fourth row, the absorbance, a, is also dimensionless and so has no units. In this row, the sample path length l has units of cm. Note also the assumptions concerning these equations, listed in the main text (dipole orientation, line broadening and mode volume).

	$\bar{\nu}$ (cm^{-1})	ω (rad s^{-1})	E (eV)
ϵ	$\frac{0.24}{\sqrt{n_{host}}}\sqrt{\epsilon_{max}C_m\delta\bar{\nu}}$	$\frac{1.05\times10^5}{\sqrt{n_{host}}}\sqrt{\epsilon_{max}C_m\delta\omega}$	$\frac{2.70\times10^{-3}}{\sqrt{n_{host}}}\sqrt{\epsilon_{max}C_m\delta E}$
α	$\frac{0.16}{\sqrt{n_{host}}}\sqrt{\alpha_{max}\delta\bar{\nu}}$	$\frac{6.92\times10^4}{\sqrt{n_{host}}}\sqrt{\alpha_{max}\delta\omega}$	$\frac{1.78\times10^{-3}}{\sqrt{n_{host}}}\sqrt{\alpha_{max}\delta E}$
κ	$\frac{0.56}{\sqrt{n_{host}}}\sqrt{\kappa_{max}\nu_0\,\delta\bar{\nu}}$	$\frac{0.56}{\sqrt{n_{host}}}\sqrt{\kappa_{max}\omega_0\,\delta\omega}$	$\frac{0.56}{\sqrt{n_{host}}}\sqrt{\kappa_{max}E\,\delta E}$
a	$\frac{0.24}{\sqrt{n_{host}}}\sqrt{\frac{a_{max}\delta\bar{\nu}}{l}}$	$\frac{1.05\times10^5}{\sqrt{n_{host}}}\sqrt{\frac{a_{max}\delta\omega}{l}}$	$\frac{2.70\times10^{-3}}{\sqrt{n_{host}}}\sqrt{\frac{a_{max}\delta E}{l}}$

the width is likely to lead to errors. The three assumptions listed immediately above also apply to the formulae listed in Table 1. In the next section, we look at a number of worked examples.

3 Worked examples

3.1 Absorbance: Nile Red in a polymer brush film

We consider first a system consisting of the dye Nile Red attached to a surface-grafted aldehyde-functional hydrophilic polymer brush scaffold. Brushes are thin films (typically <100 nm in thickness) in which polymer chains are end-tethered to an underlying substrate [35]. These surface layers have been shown to have many desirable properties [36], including increased antifouling [36] and lubricity [37] and can act as a scaffold for various small and large molecules [38], [39]. In the example presented here, a hydrophilic aldehyde functional polymer brush (PAGEO5MA) was grown from a glass cover slip [40]–[42], with a dry thickness = 40 nm, before decoration with an amino-functionalised Nile Red analogue (2-(2-Aminoethoxy) Nile Red) [43]. We have shown that PAGEO5MA can be conjugated with reactive amines through reductive amination chemistry to produce highly functionalised coatings (>80 % of available reactive sites) [40]–[42]. Further details of the synthesis and characterisation of the Nile Red analogue, the PAGEO5MA brush and Nile Red-brush system are outlined in Appendix F.

The transmittance is measured in a standard UV–VIS spectrophotometer. Usually the absorbance is calculated from the transmittance as $a = \log_{10}(I(0)/I(t))$, where $I(0)$ and $I(t)$ are the incident and transmitted intensities, respectively. However, this equation does not take into account and reflection of light by the sample, and for a highly absorbing thin film, this reflection can be substantial (in the case of the film used for Figure 2, the maximum reflection – on resonance – was ~10 %) leading to an overestimate of the absorbed power. To account for this reflected light, we need to use,

$$a = \log_{10}\left(\frac{I(0) - I(r)}{I(t)}\right). \tag{7}$$

where $I(r)$ is the reflected intensity, see Figure 6 below.

The measured absorbance of such a thin film on a glass substrate is shown in Figure 2. Note that for these data, the power lost to reflections was estimated by simulating the reflectance using a Fresnel-type calculation, a calculation that incorporated the resonance of the Nile Red dye. If this correction is not made, the absorbance is overestimated
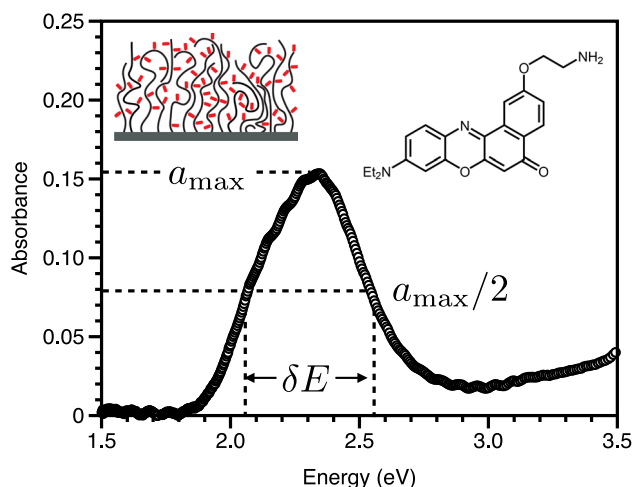
Figure 2: Absorbance of Nile Red functionalised PAGEO5MA polymer brush. Experimental data for the absorbance of a 40 nm PAGEO5MA polymer brush functionalised with Nile Red. From these data, we find the maximum absorbance to be $a_{max} \sim 0.15$, and the width to be $\delta E \sim 0.49$ eV. The inset top left shows a schematic of the dye molecules (red) incorporated into the brush. The inset top right shows the structure of the variant of Nile Red we used (for further details see Appendix F).

by 15 %. Further note that we have also ignored any possible scattering. In a future publication will discuss these important issues concerning data analysis from UV–VIS spectrophotometer measurements more fully. Since the data are in terms of eV, see Figure 2, the formula we need for the coupling strength is, see Table 1, lower right entry,

$$g_N = \frac{2.7 \times 10^{-3}}{\sqrt{n_{host}}} \sqrt{\frac{a_{max}\delta E}{l}}. \tag{8}$$

From Figure 2, the maximum absorbance is 0.15, and the width is $\delta E \sim 0.49$ eV. The polymer brush is $l = 40$ nm thick but the units we need here are cm, so the thickness is 4×10^{-6} cm, thus with $\sqrt{n_{host}} \sim 1.2$, we find $g_N = 0.31$ eV. Using this result, and the fact that $\Gamma \sim \delta E \sim 0.49$ eV, together with condition (2), we can see that provided $K < 0.75$ eV, i.e. we employ a cavity mode of width no greater than 0.75 eV, then observing the effects of strong coupling, e.g. split peaks (see Figure 1) should be possible. This estimate assumes that the mode volume is filled by the dye, i.e. that the 40 nm thick brush layer fills the mode volume. As noted above, this may be reasonable, e.g. for a particle plasmon resonance [44], [45] but will not be the case for a surface plasmon on a planar surface, or a standard Fabry–Pèrot cavity mode. Nonetheless, in these latter cases, there is considerable margin to make use of the Nile Red–doped brush since it would be easy to employ a cavity mode with a much narrower mode, for example a Fabry–Pèrot cavity might typically have $K \sim 0.1$ eV.

3.2 Extinction: TDBC in a layer-by-layer film

Our second example is based on a molecular system that has been a workhorse in strong coupling experiments, the aggregated dye TDBC [7], [46]. This dye has been extensively used because it has a strong (high oscillator strength) yet narrow transition. Various approaches to making structures containing TDBC can be employed; here, we show data based on ellipsometry of 4 layers of TDBC deposited on a glass substrate using a layer-by-layer approach [7], [47], [48].

Again, because these data are in terms of eV, see Figure 3, the formula we need for the coupling strength is in row three, right hand column of Table 1,

$$g_N = \frac{0.56}{\sqrt{n_{host}}} \sqrt{\kappa_{max}E\,\delta E}. \tag{9}$$

From Figure 3, the maximum extinction is $\kappa \sim 1.75$, the width is $\delta E \sim 0.08$ eV and the transition is at $E \sim 2.14$ eV. Again assuming $\sqrt{n_{host}} \sim 1.2$, we find $g_N = 0.25$ eV. This is comfortably greater than the TDBC linewidth $\Gamma \sim \delta E \sim 0.08$ eV so that strong coupling should be possible in a range of cavity structures. The restriction we find for the cavity linewidth using equation (2) is $K < 0.42$ eV. Note that: (i) the extinction feature is not symmetric, due to a transition on the high energy side of the main transition [45], our estimate of the width is thus an overestimate, we might expect something closer to 0.06 eV; (ii) a significantly greater density of TDBC aggregates can be achieved than has been accomplished here, see for example [49].
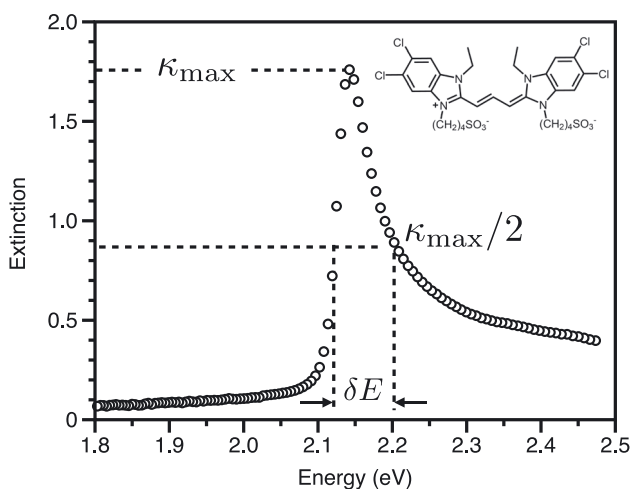

Figure 3: Real and imaginary (extinction) components of the refractive index of a TDBC layer-by-layer sample, 4 layers thick. The data are derived from ellipsometry measurements. From these data, we can estimate the transition energy to be $E = 2.14$ eV, the peak extinction to be $\kappa_{max} = 1.75$ and the FWHM of the extinction to be $\delta E = 0.08$ eV. The inset shows the chemical structure of the TDBC monomer.

3.3 Molar absorption coefficient: the C=O vibrational stretch transition

Our third example involves the C=O vibrational stretch transition in the polymer PVA. We make use of literature data from Shalbney et al. [50] (who measured the infrared transmittance associated with a thin (1.7 μm) spun film of PVA on a Ge substrate) to plot the molar absorption coefficient for this thin film, shown in Figure 4. As noted in Appendix E, the molar absorption coefficient [51], ϵ, is easily related to the transmittance and is given by,

$$\epsilon = \log_{10}\left(\frac{I_0 - I_r}{I_t}\right)\frac{1}{l\,C_m},\tag{10}$$

where again, I_0, I_r and I_t are the incident, reflected and transmitted intensities. As with the Nile Red data in the first worked example, account has been taken of the reflected power. By convention, the units for the path length, l, are cm, whilst the units for the molecular concentration, C_m, are moles per dm^{-3}, i.e. moles per litre; the units for ε are thus $dm^3\,mol^{-1}\,cm^{-1}$.

From the experiment of Shalbney et al. [50], we know the length l in this case to be $l = 1.7 \times 10^{-4}$ cm (the thickness of the PVA film), whilst the concentration of C=O bonds in PVA can be evaluated using available data [52] as 13.8 mol dm^{-3}, see also [27]. Using this information, we can convert the transmittance data of Shalbney et al. into a molar absorption coefficient, see Figure 4. We find $\epsilon_{max} \sim 426$ $dm^3\,mol^{-1}\,cm^{-1}$. Since the data are in terms of

wavenumber (cm^{-1}), see Figure 4, the formula we need for the coupling strength is, see Table 1, top left entry,

$$g_N = \frac{0.24}{\sqrt{n_{host}}}\sqrt{\epsilon_{max}C_m\delta\bar{\nu}}\tag{11}$$

From Figure 4, the width is $\delta\bar{\nu} \sim 21$ cm^{-1} so that in this case, with $\sqrt{n_{host}} \sim 1.2$, we find, $g_N = 70$ cm^{-1} so that $\Omega_R = 140$ cm^{-1}; similar to the experimentally measured value of $\Omega_R = 170$ cm^{-1}. With $\Gamma \sim \delta\bar{\nu} \sim 21$ cm^{-1}, equation (2) puts an upper linewidth on the cavity mode of 120 cm^{-1}, comfortably greater than a typical mode-width for such a system (40 cm^{-1}), see for example [53], [54].

3.4 Attenuation: R6G dye in ethanol

Our final example is that of a dye in solution, in this case R6G in ethanol at 6.89 μM. The measured attenuation coefficient is shown in Figure 5. The data are in terms of eV, see Figure 3, the formula we need for the coupling strength is in row two, right hand column of Table 1,

$$g_N = \frac{1.78 \times 10^{-3}}{\sqrt{n_{host}}}\sqrt{\alpha_{max}E\,\delta E}.\tag{12}$$

From Figure 5, the maximum attenuation is 1.6 cm^{-1}, the width is $\delta E \sim 0.14$ eV and the transition frequency is 2.34 eV. Again assuming $\sqrt{n_{host}} \sim 1.2$, we find $g_N \sim 1 \times 10^{-3}$ eV, clearly orders of magnitude below what is required for strong coupling. However, these data are for a very dilute solution, much higher concentrations are used in thin films. As an example, Hakala et al. [55] used a concentration
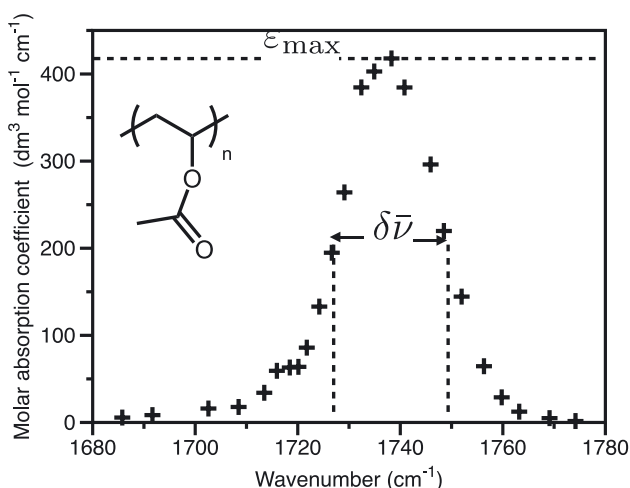

Figure 4: Experimental data for the molar absorption coefficient of a thin film of PVA on a Ge substrate. The data are adapted from [50] and have been corrected for substrate reflections etc. See also [27]. The inset shows the chemical structure of the PVA repeat unit.
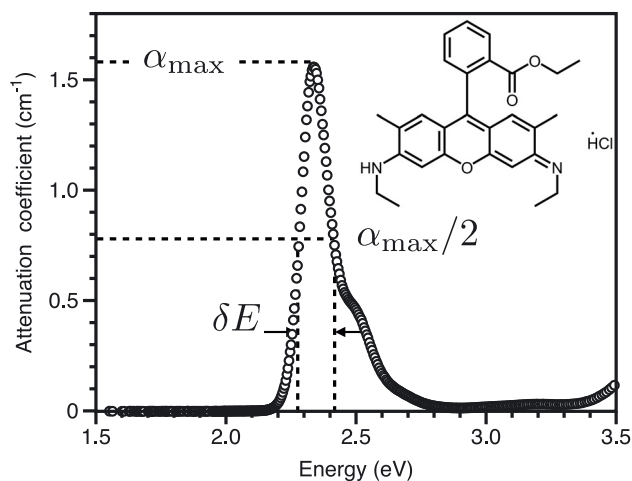

Figure 5: Attenuation of R6G in ethanol. The sample is a solution of R6G in ethanol at 6.89 μM, and the sample was held in a cuvette of 1 cm path length. The inset shows the chemical structure of R6G.

of 200 mM. If we assume no photo-physical properties are altered as the concentration increases, then this gives a value for the interaction strength of $g_N = 0.12$ eV. With a transition linewidth of $\Gamma \sim \delta E \sim 0.14$ eV, the strong coupling condition indicates that provided we can use a cavity mode with a width $K < 0.34$ eV it should be possible to observe strong coupling. The surface plasmon mode used by Hakala et al. had an estimated width of <0.05 eV, easily satisfying the required criterion.

4 Conclusions and discussion

We have presented an analysis of the strong coupling interaction between a confined light field and an ensemble of molecules that links the coupling strength to readily measured parameters. This analysis should enable, for example, a UV–VIS spectrometer to be sufficient to determine whether a material might in principle show strong coupling. This framework should thus enable the development and evaluation of new candidate molecular materials for strong coupling. Before closing, we should note some restrictions of our approach. First, we have assumed that the molecules of interest fill the mode volume – as we noted above, this is often not the case, in which situation our predictions will overestimate the extent of any strong coupling. Second, we have assumed that the vacuum electric field strength is constant across all molecules, for small (e.g. plasmonic) structures this may not be the case. Third, we have assumed we can consider a bulk material response to be appropriate. For situations where only a few molecules, perhaps only one molecule, are involved, an alternative approach will be required. Fourth, we have assumed that the resonance of interest is spectrally well isolated from other (molecular) resonances. Again, this may not be the case, especially for example in light-emitting organic materials. Fifth, we have ignored any complications due to variations in alignment between the electric field of the cavity mode and the orientation of the molecular dipole moments. Despite these approximations, we think the approach we have presented here provides a useful was to compare different candidate materials, and to estimate best-case scenarios re: the extent of strong coupling.

Appendix A: Strong coupling criteria

There are various forms for the strong coupling condition. One well-used condition is [2],

$$g_N^2 > \frac{\gamma_{\text{mol}}^2 + \gamma_{\text{cav}}^2}{2}, \tag{A1}$$

where γ_{mol} and γ_{cav} are the dephasing rates of the molecular transition and cavity field, respectively (see comment in Appendix C). A more convenient condition from an experimental point of view can be given in terms of the linewidths rather than the dephasing rates. If we note that the extent of the anti-crossing is $\Omega_R = 2g_N$ (this is also known as the Rabi frequency), and that the molecular and cavity linewidths, Γ and K, respectively, are typically twice the dephasing rates [2], [27], then we can write the strong coupling condition as [2],

$$\Omega_R = 2g_N > \frac{\Gamma + K}{2}. \tag{A2}$$

This condition is used in the present work.

Appendix B: Interaction strength in terms of dipole moment

We can make use of equation (5) for the interaction strength in terms of the dipole moment to provide the following worked example. We choose as our system the coupling of the C=O bind vibration in the polymer PVA to a planar infra-red optical microcavity mode, following the

pioneering work of Shalabney et al. [50] and Long and Simpkins [53]. Elsewhere [27] we use a transfer matrix approach to model the transmission of the bare PVA film used by Shalabney et al., [50]. Doing so we are able to determine the dipole moment to be 0.97×10^{-30} cm. For PVA, we have that $N/V = 8.33 \times 10^{27}$ m^{-3} and $\varepsilon_{\text{host}} = 2$. For the C=O resonance $\omega_0 = 3.26 \times 10^{14}$ rad s^{-3} [27]. Putting these values into (4), we find $g_N = 80$ cm^{-3}. Note that to find this value, we divided the right-hand side of (4) by $\sqrt{3}$ to take account of the random orientation of dipole moments expected in this system, see section Appendix C. This compares with the measured value [50] of $g_N \approx 85$ cm^{-3}.

Appendix C: Interaction strength and material response

$$\varepsilon(\omega) = \varepsilon_{\text{host}} + \frac{f_p\, \omega_p^2}{\omega_0^2 - \omega^2 - i\omega\gamma}, \tag{C1}$$

where f_p is the oscillator strength, $\varepsilon_{\text{host}}$ is the background permittivity and, as noted above, γ is the dephasing (loss) rate. The oscillator strength f_p is related to the dipole moment and is given by [56],

$$f_p = \frac{2\, m_e\, \omega_0}{3\, \hbar\, e^2} |\mu|^2, \tag{C2}$$

Note that equation (C2) is based on the assumption that the dipole moments are randomly oriented in space, if they aligned, i.e. they are all parallel to each other, then the factor of 3 in the denominator should be removed. We can re-write equation (C2) to find the dipole moment as,

$$|\mu| = \sqrt{\frac{3\, \hbar\, e^2}{2\, m_e\, \omega_0} f_p}. \tag{C3}$$

The parameter ω_p in (C1) is given by [57],

$$\omega_p^2 = \frac{Ne^2}{V\varepsilon_0\, m_e}, \tag{C4}$$

where N/V is the density of molecules, e is the electronic charge and m_e is the electron mass. (If the electrons were free, this ω_p would be the plasma frequency. In the materials we consider here, the electrons are not free, but the nomenclature has stuck, we can simply treat ω_p as a short cut for the parameters given in (C4).) Note that ω_p contains the density of the molecules; it is a material-specific property. Substituting (C3) and (C4) into (4), we find,

$$g_{N,\text{aligned}} = \frac{\sqrt{3}}{2} \sqrt{\frac{f_p\, \omega_p^2}{\varepsilon_{\text{host}}}}, \tag{C5}$$

However, recall that equation (4) is based on the dipole moments being aligned with the cavity field. If instead the dipole moments are randomly oriented, then the factor of $\sqrt{3}$ in (C5) needs to be removed, so that,

$$g_{N,\text{random}} = \frac{1}{2} \sqrt{\frac{f_p\, \omega_p^2}{\varepsilon_{\text{host}}}}, \tag{C6}$$

From here on when we write g_N, we will imply $g_{N,\text{random}}$ unless indicated otherwise.

In Appendix D, we transform (C6) into a version based on more easily measurable parameters. First let us note that the numerator in equation (C1) is often replaced with $f_0\, \omega_0^2$ [58]. In this case, (C6) is replaced with,

$$g_N = \frac{1}{2} \sqrt{\frac{f_0\, \omega_0^2}{\varepsilon_{\text{host}}}}, \tag{C7}$$

where now f_0 is given by,

$$f_0 = \frac{2N}{3\, V\, \varepsilon_0\, \hbar\omega_0} |\mu|^2, \tag{C8}$$

and where again the molecular dipole moments are assumed to be randomly oriented.

Appendix D: Derivation of the interaction strength in terms of the extinction coefficient

On resonance $\omega = \omega_0$ and the coefficients κ, α etc. take their maximum values. We can then write equation (C1), the permittivity using the Lorentz oscillator, as,

$$\varepsilon(\omega_0) = \varepsilon_{\text{host}} + i\frac{f_p\omega_p^2}{\gamma\omega_0}, \tag{D1}$$

and, making use of equation (C6), we can write the permittivity as,

$$\varepsilon(\omega_0) = \varepsilon_{\text{host}} + i\frac{4\, \varepsilon_{\text{host}} g_N^2}{\gamma\omega_0}, \tag{D2}$$

The extinction coefficient is the imaginary component of the refractive index, κ and, since the permittivity and refractive index are related by $\varepsilon(\omega) = (n + i\kappa)^2$, we can find an expression for κ in terms of $\varepsilon(\omega)$ by finding the imaginary part of the square root of equation (D2), i.e.

$$\kappa_{\text{max}} = \sqrt{\frac{|\varepsilon_r(\omega_0)| - \text{Re}[\varepsilon_r(\omega_0)]}{2}}. \tag{D3}$$

where $\varepsilon_r(\omega_0)$ is the real part of $\varepsilon(\omega_0)$. Using (D2) and (D3), we can write the extinction coefficient as,

$$\sqrt{2}\kappa_{\max} = \sqrt{\varepsilon_{\text{host}}\left|1 + \left(\frac{4\,g_N^2}{\gamma\,\omega_0}\right)^2\right| - \varepsilon_{\text{host}}}. \qquad (D4)$$

We chose to avoid the ultrastrong coupling regime [4], for which $g_N \geq \omega_0/10$, so that $g_N < \omega_0$ and $g_N \leq \gamma$. This allows us to use the binomial theorem to write $|\varepsilon(\omega_0)| = \left[1 + 1/2\left(4\,g_N^2/\omega_0\gamma\right)^2\right]$, so that now (D4) can be re-written to give the extinction coefficient κ as,

$$\sqrt{2}\kappa_{\max} = \sqrt{\frac{\varepsilon_{\text{host}}}{2}\left(\frac{4g_N^2}{\gamma\,\omega_0}\right)^2}. \qquad (D5)$$

Rearranging we can write the interaction strength in terms of the extinction coefficient as,

$$g_N = \frac{1}{2\sqrt{n_{\text{host}}}}\sqrt{\kappa_{\max}\,\omega_0\,\delta\omega}, \qquad (D6)$$

in which $\delta\omega \sim 2\gamma$ [27]. Note that we have assumed an isotropic distribution of dipole moments with respect to the (cavity mode) electric field. If the dipole moments are aligned with the field, then because $g_N \propto f_p$, we will need to multiply g_N in equation (D6) by $\sqrt{3}$. We show below that a very similar expression can be derived through a more formal spectroscopic approach that does not rely on the assumption that the molecular resonance is well-described by the Lorentz Oscillator model, there is simply a small change in the prefactor to equation (D6), it becomes,

$$g_N = \frac{0.56}{\sqrt{n_{\text{host}}}}\sqrt{\kappa_{\max}\,\omega_0\,\delta\omega}. \qquad (D7)$$

It is this version that we use here, and that is reproduced in Table 1.

Appendix E: Different forms of the Beer–Lambert law

Frequently, the materials of interest – e.g. dye-doped polymers or solutions – are initially characterised by measuring a transmission spectrum and from the data so acquired one of the following parameters determined: the extinction coefficient, $\kappa(\omega)$; the attenuation coefficient, $\alpha(\omega)$; the molar absorption coefficient, $\epsilon(\omega)$ and the optical density, OD. These parameters are extracted from experimental data using various (equivalent) forms of the Beer–Lambert law [59] typically using a set-up similar to that shown in Figure 6. Here we look at each version of the Beer–Lambert
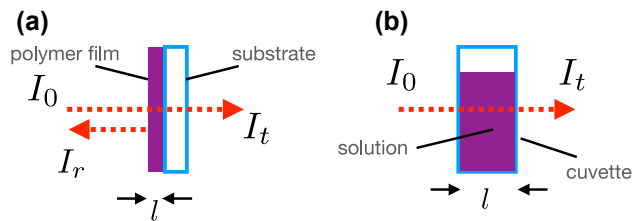

Figure 6: Typical Beer–Lambert set-up to measure the extinction of a solution/solid thin film sample. On the left (a), a thin dye-doped polymer film is shown, and on the right (b), a cuvette containing a dye solution. The intensity of light transmitted by a sample of path length (thickness) l is measured as a function of the frequency/wavelength of the light. Note that a number of precautions need to be taken to ensure transmittance data are suitable for this kind of analysis [59]. In the case of thin films of strongly absorbing molecules, account needs to be taken of the extent of any reflected power produced by the sample, see main text.

in turn. We begin by looking at the attenuation coefficient, $\alpha(\omega)$.

E.1 Attenuation coefficient, α

In terms of the attenuation coefficient, α, the Beer–Lambert law takes the form,

$$I(z) = I(0)\,e^{-\alpha z}, \qquad (E1)$$

so that,

$$\alpha = \frac{1}{t}\log_e\left(\frac{I(0)}{I(t)}\right), \qquad (E2)$$

so that, combining (E8) and (E2), we have,

$$\alpha = 2k_0\kappa. \qquad (E3)$$

Note that we take for the units of α cm^{-1}.

E.2 Molar absorption coefficient, ϵ

A common measurement parameter is the molar absorption coefficient [60], ϵ, and is given by [31], [61],

$$\epsilon = \log_{10}\left(\frac{I(0)}{I(t)}\right)\frac{1}{l\,C_m}. \qquad (E4)$$

In calculating numerical quantities, using the correct units is vital, and this applies to all of the different quantities discussed above. We will look at each of them in the notes below, but a word about the molar absorption coefficient here will be helpful. The units for the path length, l, are cm, whilst the units for the molecular concentration, C_m, are mol dm^{-3}, i.e. moles per litre, whilst the molar absorption coefficient usually has units of dm^3 mol^{-1} cm^{-1}.

E.3 Extinction coefficient, κ

With reference to Figure 6, the incident, E(0), and transmitted, E(z), electric fields are related by,

$$E(z) = E(0)\, e^{-ikz}, \tag{E5}$$

where the wavevector, k, and the complex index of refraction, $(n + i\kappa)$, of the material being measured are related through $k = k_0(n + i\kappa)$. It is the κ term in $(n' + i\kappa)$ that is responsible for the attenuation of the light, so we then have,

$$E(z) = E(0)\, e^{-k_0 \kappa z}, \tag{E6}$$

so that in terms of intensity,

$$I(z) = I(0)\, e^{-2k_0 \kappa z}, \tag{E7}$$

giving,

$$\kappa = \frac{1}{2\,k_0\,t} \log_e\left(\frac{I(0)}{I(t)}\right), \tag{E8}$$

where t is the sample thickness in metres, and in the interests of clarity, we have specified the base for the logarithm. Regarding units, κ is dimensionless, so there are no units to worry about.

E.4 Absorbance, a

The absorbance (also known as optical density, OD) is a variant of the attenuation coefficient. Then, the absorbance a is defined as,

$$a = \mathrm{OD} = \log_{10}\left(\frac{I(0)}{I(t)}\right). \tag{E9}$$

The optical density (absorbance) and the attenuation coefficient are thus related by,

$$a = \mathrm{OD} = \frac{\alpha\,t}{\log_e(10)}. \tag{E10}$$

Regarding units, a is dimensionless, so there are no units to worry about.

E.5 Interaction strength in terms of optical parameters

The equations in Table 1 are based on the different variants of the Beer–Lambert law given above.

To connect these different parameters ($\epsilon, k\,\alpha, a$) with the interaction strength, we need to express them in terms of the oscillator strength. A useful starting point is to relate the molar absorption coefficient and the oscillator strength.

Kuhn et al. [62] and Valeur and Berberan-Santos [59] provide details, and the result is,

$$\frac{f_p}{n_{\mathrm{host}}} = \frac{4\log_{10}\varepsilon_0\,c\,m_e}{N_A\,e^2} \int \epsilon(\nu)\,\mathrm{d}\nu, \tag{E11}$$

where ν is the frequency in Hz. Note that the factor of n_{host} in the denominator on the l.h.s of this equation is there to take account of the way the energy density inside the molecular material is different from that in free space, see equation (9.29) in [62]. Using standard values for the fundamental constants, the prefactor in equation (E11) can be evaluated so that and is found to be, $f_p = 1.47 \times 10^{-18} \int \epsilon(\nu)\,\mathrm{d}\nu$. Because the units for ϵ are $\mathrm{dm}^3\,\mathrm{mol}^{-1}\,\mathrm{cm}^{-1}$, we need to divide by a factor of 10 to obtain [63],

$$\frac{f_p}{n_{\mathrm{host}}} = 1.44 \times 10^{-19} \int \epsilon(\nu)\,\mathrm{d}\nu. \tag{E12}$$

In photochemistry, it is common to use a range of parameters for the spectral measurement, Hz is just one choice. Other choices include wavenumber, $\bar{\nu}$, (cm^{-1}), angular frequency, ω, ($\mathrm{rad\,s}^{-1}$) and energy, (eV). In terms of these other units, the oscillator strength is,

$$\begin{aligned}
f_p &= 4.32 \times 10^{-9}\, n_{\mathrm{host}} \int \epsilon(\bar{\nu})\,\mathrm{d}\bar{\nu} \\
&= 2.29 \times 10^{-20}\, n_{\mathrm{host}} \int \epsilon(\omega)\,\mathrm{d}\omega \\
&= 3.48 \times 10^{-5}\, n_{\mathrm{host}} \int \epsilon(\omega)\,\mathrm{d}(eV). \tag{E13}
\end{aligned}$$

Equation (E13) can often be approximated as (see [31] equation (5.40)),

$$\begin{aligned}
f_P &\approx 4.32 \times 10^{-9}\, n_{\mathrm{host}}\,\epsilon_{\mathrm{max}}\,\delta\bar{\nu} \\
&\approx 2.29 \times 10^{-20}\, n_{\mathrm{host}}\,\epsilon_{\mathrm{max}}\,\delta\omega \\
&\approx 3.48 \times 10^{-5}\, n_{\mathrm{host}}\,\epsilon_{\mathrm{max}}\,\delta(eV), \tag{E14}
\end{aligned}$$

where $\delta\bar{\nu}$, $\delta\omega$ and $\delta(eV)$ are the spectral widths (FWHM) of the extinction feature. Noting that the number density of molecules (number per cubic metre) $N/V = 10^3 C_m N_A$, where N_A is Avagadro's number, then we can use (E14) and (C4) in (C6), together with known values of physical constants, to find $e^2/\varepsilon_0 m_e = 3.18 \times 10^3$, so that,

$$\begin{aligned}
g_N &= \frac{0.24}{\sqrt{n_{\mathrm{host}}}} \sqrt{\epsilon_{\mathrm{max}}\,C_m\,\delta\bar{\nu}} \\
&= \frac{1.05 \times 10^5}{\sqrt{n_{\mathrm{host}}}} \sqrt{\epsilon_{\mathrm{max}}\,C_m\,\delta\omega} \\
&= \frac{2.70 \times 10^{-3}}{\sqrt{n_{\mathrm{host}}}} \sqrt{\epsilon_{\mathrm{max}}\,C_m\,\delta(eV)}, \tag{E15}
\end{aligned}$$

where, for clarity, the maximum (spectral peak) value of the molar absorption coefficient, ϵ_{max}, is found from transmittance data using equation (E4), the concentration C_m is in moles per litre and the spectral width of the extinction peak, $\delta\bar{\nu}, \delta\omega, \delta(eV)$ are in wavenumbers, metres, radians per second and eV (as appropriate), and n_{host} is the background refractive index, e.g. of the solvent.

Now that we have what we need for the molar absorption coefficient, we can use equations (D7), (E3) and (E10) to find similar expressions in terms of the maximum extinction coefficient, κ_{max}, the maximum absorption coefficient, α_{max}, and the maximum absorbance, a_{max}, which are related according to,

$$\epsilon_{max} C_m = \frac{\alpha_{max}}{2.3} = \frac{2\kappa_{max}\,\omega_0}{2.3 \times 10^2\,c} = \frac{a_{max}\log_e(10)}{2.3\,l}. \quad \text{(E16)}$$

where the attenuation coefficient, α, is in units of cm^{-1}, and the path length, l, is also in cm.

Appendix F: Details of the synthesis and characterisation of Nile Red analogue, PAGEO5MA brushes and the Nile Red-PAGEO5MA brush system

F.1 Materials

Sodium periodate ($\geq$99.8 %, $NaIO_4$), (3-aminopropyl)triethoxysilane (>99 %, APTES), triethylamine (99 %, NEt_3), 2-bromoisobutyryl bromide (>99 %, BiBB), copper(II) chloride (99.999 %, $CuCl_2$), ascorbic acid (>98 %, AscA), sodium cyanoborohydride (95 %, $NaBH_3CN$), dichloromethane (>99 %, DCM), diethyl ether (> = 99.8 %), N-(1-naphthyl)ethylenediamindihydrochloride (>98 %) and ammonia solution (NH_4OH, 35 %) were purchased from Sigma-Aldrich, UK and were used without further purification. 3-Diethylaminophenol (99 %, Acros Organics, UK), sodium azide (>99 %, Acros Organics, UK), sodium nitrite (>97 %, Alfa Aesar, UK), dibromoethane (98 %, Alfa Aesar, UK), hydrochloric acid (HCl, 35 wt%, Scientific Laboratory Supplies, UK), potassium carbonate (100 %, K_2CO_3, VWR, UK), petroleum ether (40–60, 95 % VWR), magnesium sulphate (dried, Fisher Scientific, UK), sodium hydroxide (>97 %, NaOH, Fisher Scientific, UK) and sodium chloride (>=99.5 %, NaCl, Fisher Scientific, UK) were also used as purchased. GEO5MA monomer was kindly donated by GEO Speciality Chemicals, UK and was used without further purification. All other solvents were purchased from Fisher Scientific, UK and were used as received unless otherwise stated herein. N,N,N′,N′′,N′′-Pentamethyldiethylenetriamine (>99 %, PMDETA) was also purchased from Fisher Scientific, UK. Deionised water (pH 6.8) was obtained using an Elga Elgastat Oprion 3A water purification system. Native oxide-coated silicon wafers were purchased from Pi-KEM, UK. Column chromatography was performed using silica gel (40–60 µm, VWR, UK) as the stationary phase, monitored by thin layer chromatography (TLC) using Merck silica gel 60 F254 plates and visualised under UV light if required. NMR spectra were recorded on a Bruker Avance III HD and chemical shifts referenced to residual solvent. Mass spectra were recorded by the University of Sheffield Mass Spectrometry facility on an Agilent 6530 Accurate Mass LC-MS QToF mass spectrometer (LCMS, high resolution) or a Waters LCT Classic (direct infusion, low resolution). 3-Diethylamino-2-nitrosophenol hydrochloride [64] and 2-Hydroxy Nile Red [65] were synthesised according to published procedures. Microscope coverslip glass slides (22 mm, 50 mm, 1.5 mm thickness) were obtained from Menzel-Gläser, Germany. Ethyl acetate (EtOAc, 99 %) and dichloromethane (DCM, 99 %) were purchased from Fisher Science and used as provided.

F.2 Preparation of 2-(2-aminoethoxy) Nile Red

(Figure 7)

F.2.1 Preparation of 2-(2-bromoethoxy) Nile Red

Our synthesis route is a version of a previously reported protocol [64]. 2-Hydroxy Nile Red (0.407 g, 1.22 mmol), potassium carbonate (1.686 g, 12.20 mmol) and anhydrous DMF (10 mL) were combined under N_2. 1,2-Dibromoethane (3.2 mL, 37.13 mmol) was added to the stirred mixture and the reaction was heated to 65 °C. The reaction was tracked by TLC (1:1 EtOAc/pet ether) and cooled to 20 °C after 1 h 10 min. DCM (50 mL) and deionised water (50 mL) were added, the layers separated and the organic layer washed with DI water (2×30 mL), the aqueous washings back-extracted with DCM (3×30 mL) and the combined organic layers washed with brine (80 mL), dried over $MgSO_4$ and concentrated in vacuo. The crude solid was subjected to flash chromatography (1:1 EtOAc/pet ether, rising to 2:1 once fast moving impurities had eluted) yielding 2-(2-bromoethoxy) Nile Red as a purple solid (0.292 g, 0.66 mmol, 54 %): ^{1}H NMR (400 MHz, $CDCl_3$) δ 8.27 (d, J = 8.7 Hz, 1H), 8.10 (d, J = 2.6 Hz, 1H), 7.64 (d, J = 9.1 Hz, 1H), 7.23 (dd, J = 8.7, 2.6 Hz, 1H), 6.70 (dd, J = 9.1, 2.8 Hz, 1H), 6.50 (d, J
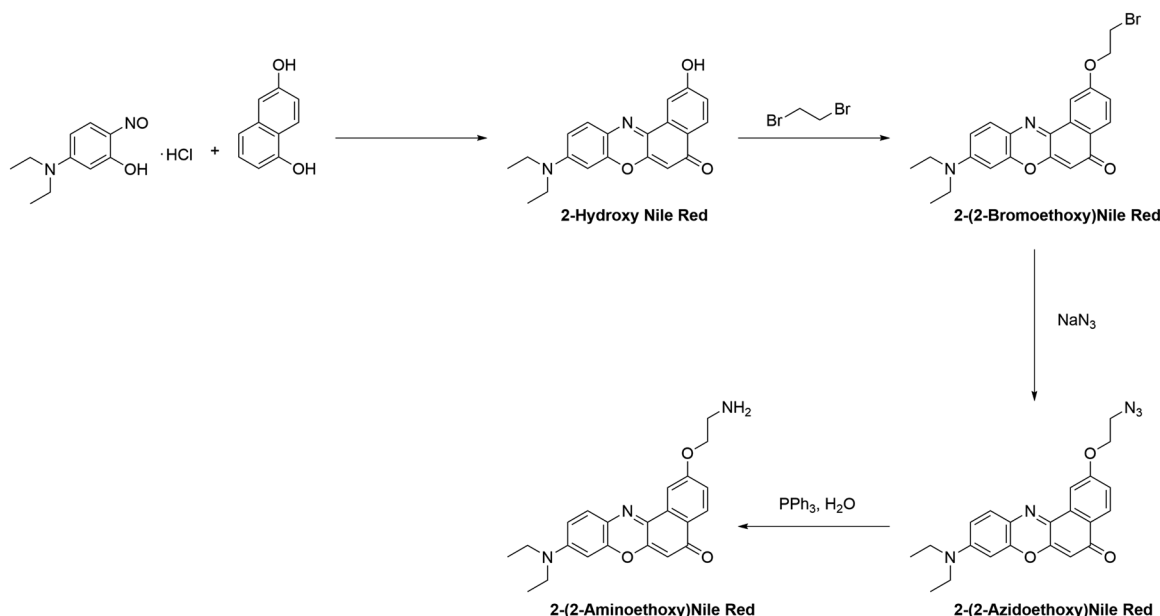
Figure 7: Synthesis of 2-(2-aminoethoxy) Nile Red.

= 2.7 Hz, 1H), 6.34 (s, 1H), 4.54 (t, J = 6.2 Hz, 2H), 3.76 (t, J = 6.2 Hz, 2H), 3.50 (q, J = 7.1 Hz, 4H), 1.29 (t, J = 7.1 Hz, 6H); ^{13}C{^{1}H} NMR (100 MHz, CDCl$_3$) δ 183.09, 160.67, 152.09, 150.82, 146.87, 139.67, 134.08, 131.10, 127.91, 126.17, 124.71, 118.32, 109.61, 106.65, 105.28, 96.28, 77.37, 77.26, 77.05, 76.73, 68.06, 45.11, 28.97, 12.65; HRMS (ESI): m/z 441.0818 [M + H]$^+$, calculated for C$_{22}$H$_{22}$N$_2$O$_3$Br$^+$ 441.0808.

F.2.2 Preparation of 2-(2-azidoethoxy) Nile Red

Our synthesis route is a version of a previously reported protocol [65]. 2-(2-Bromoethoxy) Nile Red (0.290 g, 0.657 mmol) and NaN$_3$ (0.064 g, 0.984 mmol) were dissolved in anhydrous DMF (10 mL). The mixture was stirred at 80 °C under N$_2$ for 20 h and cooled to RT. EtOAc (50 mL) was added and the solution washed with 3M NaOH (3 × 50 mL) and brine (50 mL). The organics were dried over MgSO$_4$ and concentrated in vacuo, yielding 2-(2-azidoethoxy) Nile Red as a purple solid (0.261 g, 0.647 mmol, 98 %). This was used without further purification: ^{1}H NMR (400 MHz, CDCl$_3$) δ = 8.24 (d, J = 8.7 Hz, 1H), 8.05 (d, J = 2.7 Hz, 1H), 7.58 (d, J = 9.0 Hz, 1H), 7.20 (dd, J = 8.7, 2.6 Hz, 1H), 6.66 (dd, J = 9.1, 2.7 Hz, 1H), 6.45 (d, J = 2.7 Hz, 1H), 6.30 (s, 1H), 4.38 (t, J = 4.9 Hz, 2H), 3.71 (t, J = 5.0 Hz, 2H), 3.48 (q, J = 7.1 Hz, 4H), 1.28 (t, J = 7.1 Hz, 6H) ppm; ^{13}C^{1}H NMR (100 MHz, CDCl$_3$) δ = 183.11, 160.80, 152.09, 150.82, 146.87, 139.69, 134.08, 131.09, 127.89, 126.16, 124.71, 118.38, 109.60, 106.44, 105.29, 96.28, 67.24, 50.18, 45.10, 12.64 ppm; HRMS (ESI): m/z 404.1722 [M + H]$^+$, calcd for C$_{22}$H$_{22}$N$_5$O$_3^+$ 404.1717.

F.2.3 Preparation of 2-(2-aminoethoxy) Nile Red

Our synthesis route is a version of a previously reported protocol [43]. 2-(2-Azidoethoxy) Nile Red (0.030 g, 0.074 mmol) and PPh$_3$ (0.029 g, 0.111 mmol) were dissolved in anhydrous THF (1 mL) and stirred under N$_2$ for 1 h. DI water (5 drops) was added, the mixture stirred for 18 h and the solvent removed in vacuo. The crude material was subjected to flash chromatography (DCM/methanol (5 %)/NH$_4$OH(1 %) rising to 10 % methanol once fast moving impurities had eluted) yielding 2-(2-aminoethoxy) Nile Red as a purple solid (0.022 g, 0.058 mmol, 78 %): ^{1}H NMR (400 MHz, CDCl$_3$) δ 8.20 (d, J = 8.7 Hz, 1H), 8.03 (d, J = 2.6 Hz, 1H), 7.55 (d, J = 9.1 Hz, 1H), 7.16 (dd, J = 8.7, 2.6 Hz, 1H), 6.62 (dd, J = 9.1, 2.7 Hz, 1H), 6.41 (d, J = 2.7 Hz, 1H), 6.27 (s, 1H), 4.20 (t, J = 5.2 Hz, 2H), 3.45 (q, J = 7.1 Hz, 4H), 3.18 (t, J = 5.2 Hz, 2H), 1.26 (t, J = 7.1 Hz, 7H), MS (ESI): m/z 378.2 [M + H]$^+$, calculated for C$_{22}$H$_{24}$N$_3$O$_3^+$ 378.2.

F.3 Surface functionalisation of glass cover slips and silicon wafers with ARGET ATRP initiator

Functionalisation of planar silicon wafers and glass cover slips with ARGET ATRP initiator moieties was carried out following an experimental protocol reported by Brotherton et al. [41]. Silicon (100) wafers were cut into small pieces (1 × 1 cm^2) before being UV-ozone cleaned for 30 min using a Bioforce Nanosciences ProCleaner. The wafers were then placed in an open Petri dish along with a 3 mL glass vial

containing 100 μL APTES. The Petri dish was then placed in a desiccator, which was subsequently sealed and placed under vacuum. Vapour deposition was allowed to proceed for 30 min before the surfaces were removed and placed in a 110 °C oven for 30 min. The wafers were then functionalized by immersion in DCM followed by sequential addition of NEt_3 (final concentration = 0.2 mM) and BiBB (final concentration = 0.2 mM), allowing the amidation reaction to proceed for 1 h at 22 °C. Finally, the initiator-functionalised silicon wafers were rinsed extensively with ethanol and DI water, before drying under a stream of compressed air.

F.4 Grafting of PGEO5MA brushes via surface-initiated ARGET ATRP from initiator functionalised surfaces

Following surface functionalisation with initiator moieties, surface initiated-activators regenerated via electron transfer, and atom transfer radical polymerisation (SI-ARGET ATRP) was employed to grow PGEO5MA homopolymer brushes from each surface. We have recently reported a detailed description of the protocol synthesis [41]. Briefly, a GEO5MA:$CuCl_2$:PMDETA:ascorbic acid molar ratio of 1000:1:5:5 was used. Deionised water was the solvent with a final monomer concentration of 45 % v/v. Polymerisations were allowed to proceed for 1 h at 22 °C in all cases. Each PGEO5MA-functionalized wafer or cover slip was subsequently rinsed thoroughly with ethanol and DI water and then dried using a stream of N_2 gas.

F.5 Selective oxidation of *cis*-diol-functional PGEO5MA brushes for the synthesis of aldehyde-functional PAGEO5MA brushes

Following our previously reported experimental protocol for selective oxidation of surface-grafted polymer brushes [41], PGEO5MA-functionalized planar silicon wafers were immersed in a 3.0 mg mL^{-1} aqueous solution of $NaIO_4$ for 30 min at 22 °C, targeting a degree of oxidation of 100 % in all cases. Each aldehyde functional 'PAGEO5MA' functionalized silicon wafer was subsequently rinsed thoroughly with DI water and then dried using a stream of compressed air.

F.6 Preparation of Nile Red-PAGEO5MA brushes from aldehyde-functional PAGEO5MA brushes via reductive amination

Oxidised PAGEO5MA brushes were functionalized with 2-(2-aminoethoxy) Nile Red via reductive amination. A

1.0 g dm^{-3} solution of this amine dye was prepared in methanol before addition of a 1.5 × molar excess of $NaBH_3CN$. Brushes were immersed in this solution and allowed to react for 24 h at 50 °C. The resulting Nile Red-PAGEO5MA brushes were rinsed extensively with methanol, ethanol and deionised water and then dried under a stream of compressed air.

F.7 Characterisation of dry polymer brushes

F.7.1 Ellipsometry

Ellipsometry measurements of dry polymer brushes grown from planar silicon wafers were performed using a J. A. Woollam M-2000 V ellipsometer at a fixed angle of incidence of 75° normal to the sample surface in air at 20 °C. A two-layer model consisting of a native oxide layer and Cauchy layer was used to model the data. Data analysis and modelling were performed using Woollam CompleteEase software. Cauchy constants of $A_n = 1.459$, $B_n = 0.006$ and $C_n = 0$ were used. The ellipsometer set-up allowed a relatively large sampling area of approximately 0.5 cm × 1 cm, which corresponds to around 50 % of the total area of each brush sample. Brushes grown from glass were assumed to be of equal thickness to that grown from silicon wafers present in the same reaction vial.

F.7.2 X-ray photoelectron spectroscopy (XPS)

XPS analysis of dry polymer brushes grafted from planar silicon wafers was performed using a Kratos Axis Supra spectrometer. Step sizes of 0.50 and 0.10 eV were used to record survey and high-resolution C1s, O1s and N1s spectra, respectively. In each case, spectra were recorded from at least two separate areas for each surface-grafted brush. The XPS data were analysed using Casa XPS software. All binding energies were calibrated with respect to the C1s saturated hydrocarbon peak at 285.0 eV. The degree of functionalisation of the brush was determined by comparing the nitrogen/oxygen atomic ratios using the high resolution spectra and was found to be = 82 ± 5 %.

F.7.3 UV-visible absorption

Measurements were performed on Cary50 spectrophotometer (Agilent Technologies, USA) with a baseline transmission through a cuvette prior to measurements. Nile Red functionalised PAGEO5MA brushes on glass coverslips were positioned in a plastic cuvette and absorbance at normal incidence measured over a 300−800 nm wavelength range.

A background subtraction of a glass coverslips (measured separately) was performed post measurement. For the R6G solutions, transmittance was measured over a $200-800$ nm wavelength range in a quartz cuvette. The concentrations of the dyes were selected to ensure suitable transmittance was measured.

References

[1] T. W. Ebbesen, "Hybrid light−matter states in a molecular and material science perspective," *Acc. Chem. Res.*, vol. 49, no. 11, p. 2403, 2016.

[2] M. S. Rider and W. L. Barnes, "Something from nothing: linking molecules with virtual light," *Contemp. Phys.*, vol. 62, no. 4, p. 217, 2021.

[3] D. G. Lidzey, D. D. C. Bradley, T. Virgil, A. Armitage, M. S. Skolnick, and S. Walker, "Room temperature polariton emission from strongly coupled organic semiconductor microcavities," *Phys. Rev. Lett.*, vol. 82, no. 16, p. 3316, 1999.

[4] A. F. Kockum, A. Miranowicz, S. De Liberato, S. Savasta, and F. Nori, "Ultrastrong coupling between light and matter," *Nat. Rev. Phys.*, vol. 1, no. 1, p. 19, 2019.

[5] X. Zhong, *et al.*, "Non-radiative energy transfer mediated by hybrid light-matter states," *Angew. Chem., Int. Ed.*, vol. 55, no. 21, p. 6202, 2016.

[6] K. Georgiou, P. Michetti, L. Gai, M. Cavazzini, Z. Shen, and D. G. Lidzey, "Control over energy transfer between fluorescent BODIPY dyes in a strongly coupled microcavity," *ACS Photonics*, vol. 5, no. 1, p. 258, 2017.

[7] M. Balasubrahmaniyam, A. Simkhovich, A. Golombek, G. Sandik, G. Ankonina, and T. Schwartz, "From enhanced diffusion to ultrafast ballistic motion of hybrid light−matter excitations," *Nat. Mater.*, vol. 22, no. 3, p. 338, 2023.

[8] D. Sidler, C. Schäfer, M. Ruggenthaler, and A. Rubio, "Polaritonic chemistry: collective strong coupling implies strong local modification of chemical properties," *J. Phys. Chem. Lett.*, vol. 12, no. 1, p. 508, 2020.

[9] K. Hirai, J. A. Hutchison, and H. Uji-i, "Recent progress in vibropolaritonic chemistry," *ChemPlusChem*, vol. 85, no. 9, p. 1981, 2020.

[10] X. Li, A. Mandal, and P. Huo, "Cavity frequency-dependent theory for vibrational polariton chemistry," *Nat. Commun.*, vol. 12, no. 1, p. 1315, 2021.

[11] J. A. Campos-Gonzalez-Angulo, Y. R. Poh, M. Du, and J. Yuen-Zhou, "Swinging between shine and shadow: theoretical advances on thermally activates vibropolaritonic chemistry", arXiv:2212.04017, 2022.

[12] L. Chen, A. P. Fidler, A. M. McKillop, and M. L. Weichman, "Exploring the impact of vibrational cavity coupling strength on ultrafast CN + c-CH6H12 reaction dynamics," arXiv:2301.19133, 2023.

[13] T. Khazanov, S. Gunasekaran, A. George, R. Lomlu, S. Mukherjee, and A. J. Musser, "Embrace the darkness: an experimental perspective on organic exciton−polaritons," *Chem. Phys. Rev.*, vol. 4, no. 4, p. 041305, 2023.

[14] F. Herrera and J. Owrutsky, "Molecular polaritons for controlling chemistry with quantum optics," *J. Chem. Phys.*, vol. 152, no. 10, p. 100902, 2020.

[15] J. Fregoni, F. J. Garcia-Vidal, and J. Feist, "Theoretical challenges in polaritonic chemistry," *ACS Photonics*, vol. 9, no. 1, p. 1096, 2022.

[16] J. Feist, A. I. Fernández-Domínguez, and F. J. García-Vidal, "Macroscopic QED for quantum nanophotonics: emitter-centered modes as a minimal basis for multiemitter problems," *Nanophotonics*, vol. 10, no. 1, p. 477, 2021.

[17] I. Sokolovskii, R. H. Tichauer, J. Feist, and G. Groenhof, "Enhanced excitation energy transfer under strong light-matter coupling: insights from multi-scale molecular dynamics simulations," arXiv:2209.07309, 2022.

[18] A. M. Berghuis, *et al.*, "Controlling exciton propagation in organic crystals through strong coupling to plasmonic nanoparticle arrays," *ACS Photonics*, vol. 9, no. 7, pp. 2263−2272, 2022.

[19] Y. Zhu, D. J. Gauthier, S. Morin, Q. Wu, H. Carmichael, and T. Mossberg, "Vacuum Rabi splitting as a feature of linear-dispersion theory: analysis and experimental observations," *Phys. Rev. Lett.*, vol. 64, no. 21, p. 2499, 1990.

[20] C. Weisbuch, M. Nishioka, A. Ishikawa, and Y. Arakawa, "Observation of the coupled exciton-photon mode splitting in a semiconductor quantum microcavity," *Phys. Rev. Lett.*, vol. 69, no. 23, p. 3314, 1992.

[21] M. Barra-Burillo, *et al.*, "Microcavity phonon polaritons from the weak to the ultrastrong phonon−photon coupling regime," *Nat. Commun.*, vol. 12, no. 1, p. 6206, 2021.

[22] W. L. Barnes, "Particle plasmons: why shape matters," *Am. J. Phys.*, vol. 84, no. 8, p. 593, 2016.

[23] K. Ujihara, "Spontaneous emission and the concept of effective area in a very short optical cavity with plane-parallel dielectric mirrors," *Jpn. J. Appl. Phys.*, vol. 30, no. 5B, p. L901, 1991.

[24] P. Lalanne, W. Yan, K. Vynck, C. Sauvan, and J.-P. Hugonin, "Light interaction with photonic and plasmonic resonances," *Laser Photonics Rev.*, vol. 12, no. 5, p. 1700113, 2018.

[25] V. M. Agranovich, M. Litinskaia, and D. G. Lidzey, "Cavity polaritons in microcavities containing disordered organic semiconductors," *Phys. Rev. B*, vol. 67, no. 8, p. 085311, 2003.

[26] A. Tsargorodska, *et al.*, "Strong coupling of localized surface plasmons to excitons in light-harvesting complexes," *Nano Lett.*, vol. 16, no. 11, p. 6850, 2016.

[27] W. L. Barnes, "Molecular strong coupling: evaluating dipole oscillator and cavity field parameters," *Physica Scripta*, 2023, Submitted for publication.

[28] C. On, E. Tanyi, E. Harrison, and M. Noginov, "Effect of molecular concentration on spectroscopic properties of poly(methyl methacrylate) thin films doped with rhodamine 6G dye," *Opt. Mater. Express*, vol. 7, no. 12, p. 4286, 2017.

[29] A. B. Djurišić, T. Fritz, and K. Leo, "Modeling the optical constants of organic thin films: application to 3,4,9,10-perylenetetracarboxylic dianhydride (PTCDA)," *Opt. Commun.*, vol. 183, no. 1, p. 123, 2000.

[30] A. Dutta, V. Tiainen, H. A. Qureshi, L. Duarte, and J. J. Toppari, "Modeling optical constants from the absorption of organic thin films using a modified Lorentz oscillator model," *Opt. Mater. Express*, vol. 12, no. 7, p. 2855, 2022.

[31] N. J. Turro, *Modern Molecular Photochemsitry*, Sausalito, California, University Science Books, 1991.

[32] G. Zengin, *et al.*, "Evaluating conditions for strong coupling between nanoparticle plasmons and organic dyes using scattering and absorption spectroscopy," *J. Phys. Chem. C*, vol. 120, no. 37, p. 20588, 2016.

[33] S. Gunasekaran, R. F. Pinard, and A. J. Musser, "Continuum model of strong light-matter coupling for molecular polaritons," arXiv:2308.08744, 2023.

[34] J. Mooney and P. Kambhampati, "Get the basics right: jacobian conversion of wavelength and energy scales for quantitative analysis of emission spectra," *J. Phys. Chem. Lett.*, vol. 4, no. 4, p. 3316, 2013.

[35] W. J. Brittain and S. Minko, "A structural definition of polymer brushes," *J. Polym. Sci., Part A: Polym. Chem.*, vol. 45, no. 16, p. 3505, 2007.

[36] M. A. C. Stuart, *et al.*, "Emerging applications of stimuli-responsive polymer materials," *Nat. Mater.*, vol. 9, no. 2, p. 101, 2010.

[37] J. Klein, D. Perahia, and S. Warburg, "Forces between polymer-bearing surfaces undergoing shear," *Nature*, vol. 352, no. 6331, p. 143, 1991.

[38] H. Jiang and F.-J. Xu, "Biomolecule-functionalized polymer brushes," *Chem. Soc. Rev.*, vol. 42, no. 8, p. 3394, 2013.

[39] C. E. Neri-Cruz, F. M. E. Teixeira, and J. E. Gautrot, "A guide to functionalisation and bioconjugation strategies to surface-initiated polymer brushes," *Chem. Commun.*, vol. 59, no. 49, p. 7534, 2023.

[40] E. E. Brotherton, C. P. Jesson, N. J. Warren, M. J. Smallridge, and S. P. Armes, "New aldehyde-functional methacrylic water-soluble polymers," *Angew. Chem., Int. Ed.*, vol. 60, no. 21, p. 12032, 2021.

[41] E. E. Brotherton, E. C. Johnson, M. J. Smallridge, D. B. Hammond, G. J. Leggett, and S. P. Armes, "Hydrophilic aldehyde-functional polymer brushes: synthesis, characterization, and potential bioapplications," *Macromolecules*, vol. 56, no. 5, p. 2070, 2023.

[42] E. C. Johnson, *et al.*, "Adsorption of aldehyde-functional diblock copolymer spheres onto surface-grafted polymer brushes via dynamic covalent chemistry enables friction modification," *Chem. Mater.*, vol. 35, no. 15, p. 6109, 2023.

[43] I. Tosi, *et al.*, "Excitation dynamics in hetero-bichromophoric calixarene systems," *ChemPhysChem*, vol. 17, no. 11, p. 1686, 2016.

[44] N. T. Fofang, T. H. Park, O. Neumann, N. A. Mirin, P. Nordlander, and N. J. Halas, "Plexcitonic nanoparticles: plasmon−Exciton coupling in Nanoshell−J-aggregate complexes," *Nano Lett.*, vol. 8, no. 10, p. 3481, 2008.

[45] M. J. Gentile and W. L. Barnes, "Hybridised exciton−polariton resonances in core−shell nanoparticles," *J. Opt.*, vol. 19, no. 3, p. 035003, 2017.

[46] J. Bellessa, C. Bonnand, J. C. Plenet, and J. Mugnier, "Strong coupling between surface plasmons and excitons in an organic semiconductor," *Phys. Rev. Lett.*, vol. 93, no. 3, p. 036404 2004.

[47] M. Bradley, J. Tischler, and V. Bulović, "Layer-by-Layer J-aggregate thin films with a peak absorption constant of 106 cm^{-1}," *Adv. Mater.*, vol. 17, no. 15, p. 1881, 2005.

[48] M. S. Bradley and V. Bulović, "Intracavity optical pumping of J-aggregate microcavity exciton polaritons," *Phys. Rev. B*, vol. 82, no. 3, p. 033305, 2010.

[49] M. J. Gentile, S. A. R. Horsley, and W. L. Barnes, "Localized exciton−polariton modes in dye-doped nanospheres: a quantum approach," *J. Opt.*, vol. 18, no. 1, p. 015001, 2015.

[50] A. Shalabney, J. George, J. Hutchison, G. Pupillo, C. Genet, and T. W. Ebbesen, *Nat. Commun.*, vol. 6, no. 1, p. 1, 2015.

[51] Note that this is often called the molar extinction coefficient, but molar absorption coefficient is the correct term, see[66].

[52] National Center for Biotechnology Information. *PubChem Compound Summary for, Ployvinyl acetate*. Retrieved March 26, 2024 from https://pubchem.ncbi.nih.gov/compound/Polyvinylacetate.

[53] J. P. Long and B. S. Simpkins, "Coherent coupling between a molecular vibration and fabry−perot optical cavity to give hybridized states in the strong coupling limit," *ACS Photonics*, vol. 2, no. 1, p. 130, 2015.

[54] K. S. Menghrajani and W. L. Barnes, "Strong coupling beyond the light-line," *ACS Photonics*, vol. 7, no. 9, p. 2448, 2020.

[55] T. K. Hakala, *et al.*, "Vacuum Rabi splitting and strong-coupling dynamics for surface-plasmon polaritons and rhodamine 6G molecules," *Phys. Rev. Lett.*, vol. 103, no. 5, p. 053602, 2009.

[56] L. Novotny and B. Hecht, *Principles of Nano-Optics*, 1st ed. Cambridge, UK, Cambridge University Press, 2006.

[57] C. F. Bohren and D. R. Huffman, *Absorption and Scattering of Light by Small Particles*, Weinheim, Wiley VCH, 2004.

[58] This is usually done for convenience, the molecular resonance frequency ω_0 is accessible through experiment, whilst ω_p is not.

[59] B. Valeur and M. N. Berberan-Santos, *Molecular Fluorescence: Principles and Applications*, 2nd ed. Weinheim, Wiley VCH, 2012.

[60] It is often referred to as the molar extinction coefficient, but this is not the approved term [66].

[61] P. Atkins and R. Frediman, *Molecular Quantum Mechanics*, 4th ed. Oxford University Press, 2005.

[62] H. Kuhn, H.-D. Försterling, and D. H. Waldeck, *Principles of Physical Chemistry*, 2nd ed. New Jersey, Wiley, 2009.

[63] For an alternative derivation based on the Einstein coefficients, see [67].

[64] D. W. Brousmiche, *et al.*, "Fluorescence resonance energy transfer in novel multiphoton absorbing dendritic structures," *J. Phys. Chem. B*, vol. 108, no. 25, p. 8592, 2004.

[65] G. Ghini, *et al.*, "Towards a general organogelator: combining a versatile scaffold and an efficient linking process," *Soft Matter*, vol. 5, no. 9, p. 1863, 2009.

[66] S. E. Braslavsky, "Glossary of terms used in photochemistry, 3rd edition (IUPAC Recommendations 2006)," *Pure Appl. Chem.*, vol. 79, no. 3, p. 293, 2007.

[67] T. L. T. L. Weatherly and Q. Williams, *Methods of Experimental Physics − Molecular Spectroscopy*, vol. 3, D. Williams, Ed., New York, Academic Press, 1962.